Ceramics International 43 (2017) 5020–5031

Contents lists available at ScienceDirect

Ceramics International

journal homepage: www.elsevier.com/locate/ceramint

Castable systems designed with powders reclaimed from dismantled steel induction furnace refractory linings

Abílio P. Silva[a], Ana M. Segadães[b,*], Rogério A. Lopes[c]

[a] Centre for Mechanical and Aerospace Science and Technologies (C-MAST-UBI), Universidade da Beira Interior, Rua Marquês d'Ávila e Bolama, 6201-001 Covilhã, Portugal
[b] Dept. Materials and Ceramics Engineering (CICECO), University of Aveiro, 3810–193 Aveiro, Portugal
[c] DURITCAST SA, 3750–753 Travassô, Portugal

ARTICLE INFO

Keywords:
Spinel-bonded Refractory
Industrial waste
Recycling
Powders
Particle size distribution
Casting

ABSTRACT

Despite environmental pressures and intrinsic recycling potential, spent refractories waste is generally considered an economically unattractive waste stream. This work proposes an upgraded view of the debris recovered from dismantled spinel-bonded high-alumina linings of steel induction furnaces, demonstrating that it can be reused in the form of vibratable and self-flowing castable systems. The recovered material retains the microstructural distribution of in situ spinel formation without the corresponding disruptive expansion, mirroring the use of pre-formed spinel without the onus of a pre-firing. The mechanical performance after firing was found to be always best for the self-flowing system, which is also less affected by changes in added-water content. There is potential for large usages of cleaned waste (50–60 wt%), which helps reducing the supply risk for major refractory primary raw materials as well as landfilling costs.

1. Introduction

Refractory materials are used in the linings of high temperature vessels in a variety of industrial processes with strong impact in world economics, besides and beyond the obvious heavy-duty metal, glass, ceramics, petrochemical and chemical industrial processing. Being a key supplier to many other industries, improvements in the refractories industry have a significant bearing on cost savings in sustainable manufacturing of everyday life products. Just as an example, improved design and installation enabled a 75% reduction in refractory usage in steelmaking, from 60 kg/t in 1950 to 15 kg/t in 2014 [1–3].

The major users of refractories still are the iron-and-steel and the cement industries, which respectively are accountable for the consumption of 65–75% and 8–12% of the annual production of refractories [1]. With the global steel market growing at ~9% per year [4], the world demand for refractories in 2016 was estimated at 46.3 million metric tons [2].

The production of refractory linings is expensive mostly due to high raw materials costs and energy requirements. The past decades have also witnessed increased market dependency in major refractory primary raw materials. Twenty different raw materials were identified as critical (i.e. facing supply risks) in the Ad-hoc European Union working group report [5], among which graphite and magnesite. Other refractory raw materials like bauxite and silica, although non critical, were identified also as in risk. This has led to international recommendations emphasizing the need to reduce the demand on primary raw materials, promote substitution and increase recycling rates, both to alleviate supply risks and limit environmental impact through savings in energy demand [6–11].

Spent refractories are already recycled, namely into inert aggregates, insulating powders, soil conditioners or abrasives, which can translate into important savings in landfill fees. However, for higher added value applications the waste stream is generally considered economically unattractive, especially due to geographic scattering of waste sources, hence availability and transportation costs. Thus, the recycling strategy heavily depends on the economic viability of the recycling process (particularly milling and separation efficiency) rather than the recyclability of the refractory (value added to the recycled material as substitute raw material). Nevertheless, recycling spent refractories as secondary refractory raw materials meets both of those objectives and helps reducing production costs. As such, it has become a challenge to industry and Academia alike.

The incorporation of similar industrial waste materials into clay-based formulations for construction ceramics is rather successful [12,13] but designing refractories from industrial waste requires the identification of critical impurities and the control of their reactions as

* Corresponding author.
E-mail address: segadaes@ua.pt (A.M. Segadães).

http://dx.doi.org/10.1016/j.ceramint.2017.01.012
Received 28 October 2016; Received in revised form 18 December 2016; Accepted 4 January 2017
Available online 08 January 2017
0272-8842/ © 2017 Elsevier Ltd and Techna Group S.r.l. All rights reserved.

the temperature changes, to improve stiffness, toughness and resistance to thermal shock and corrosion [3]. The scientific literature provides examples of research works on refractories, concerned with diffusion profiles, microstructural changes and the effect of minor components [14,15]. In many cases, phase equilibrium diagrams can be used to foresee the reactions tendency to completion and are described as a powerful tool to guide the choice of compositions and processing parameters [13].

Industrial case studies can also be found in the literature, mostly aimed at reducing landfilling of spent refractories through higher added value reuses or in-house recycling [16–24]. Spent high alumina refractories can be reused in the production of Portland cement (~12% addition to virgin raw mixes) [16] and the incorporation of recycled material in new refractories is found to be generally economically feasible, although the increase in added-water requirements in the case of castables, for comparable flowability [18], and the presence of slag impurities (SiO_2 and CaO) might hinder some of the technological properties. In most cases, particularly with basic refractories, the need to keep the impurities level at the required minimum might call for costly separation processes or heat treatments of the refractory scrap.

This work aims to further the knowledge on the technical reuse of materials from dismantled industrial furnace monolithic linings. In particular, the study focus on a steel melting induction furnace (carbon and alloyed cast steels) whose spinel-bonded high-alumina refractory working lining usually withstands 60–90 runs (4 t of steel per run) at a peak operating temperature that can reach 1700 °C. At the end of life, the working lining is manually dismantled and the resulting debris (stones and powders) is sent to landfill (~20 t per year). The generally outstanding thermo-mechanical properties, extended service life and chemical resistance of spinel-bonded high-alumina castables is attributed to fine and well dispersed $MgAl_2O_4$ grains, which, if formed in situ by the reaction between MgO and Al_2O_3 in the castable matrix, can increase slag corrosion resistance over that of castables containing pre-formed spinel [14,15]. However, the in situ spinel formation is accompanied by a significant expansion, which can lead to microcracking and, hence, further slag infiltration. It is envisaged that the use in new formulations of granulates reclaimed from spent spinel-bonded high-alumina linings might be doubly beneficial, as they would retain the microstructural distribution of in situ spinel without the corresponding disruptive expansion, just like using pre-formed spinel without the onus of a pre-firing.

2. Experimental

The original refractory working lining (RA) is a spinel-bonded high-alumina dry ramming mix with a nominal 86 wt% Al_2O_3 and 13 wt% MgO, as specified by the supplier. The refractory scrap from the dismantled lining was collected and used as raw material throughout this work, as well as the commercial refractory, for properties comparison.

Chemical analysis was carried out by area on representative polished samples using scanning electron microscopy (SEM, Hitachi S-3400N) with energy dispersive X-ray probe (EDX, Brucker Quantax 400), after carbon coating.

The refractory scrap was manually separated into two colour-based lots, which were then ground in a SiC-W jaw crusher (Retsch BB 200). The particle size distributions (PSD) and specific surface areas (SSA) of the various powders were characterized by laser diffraction (Coulter LS 200). Helium pycnometry (Micromeritics AccuPyc 1330) was used to obtain the corresponding densities.

The particle size distributions were used to separate the powders into particle size classes and the Elkem Materials Mix Analyzer software (EMMA, Elkem AS 2012, version 3.5.2) was used to manipulate the combination of particle size classes so that a PSD with a desired Andreasen modulus, q, could be obtained [25].

The original virgin refractory raw material and the powder mixtures with designed PSD were mixed with 5 wt% water, in a planetary mixer (Retsch PM 4, for 5 min at 100 rpm) with alumina balls. With the wet mixtures, prismatic bars (5×5×55 mm^3) were cast into a double effect (floating) stainless steel casting die and uniaxially pressed at 100 MPa. The resulting test-pieces were dried (110 °C, 24 h) in a Carbolite oven. The dilatometric behaviour was characterized using a DIL801L Bärh dilatometer in air (10 °C/min heating rate, up to 1500 °C). Based on the dilatometry results, groups of five test-pieces were sintered at 1200, 1350 and 1500 °C in a Termolab furnace (5 °C/min heating rate, 30 min dwell at maximum temperature).

Sintered test-pieces were characterized in terms of firing linear change and mechanical strength (Zwick 1435 testing machine, 5 kN load cell, 2 mm/min constant crosshead speed), both as three-point bending modulus of rupture (MoR, 40 mm roller span, 5 mm roller radius) and in uniaxial compression (the best five MoR broken pieces were used, after side cutting and grinding to ensure parallelism).

Apparent porosity, bulk density and water absorption were deter-

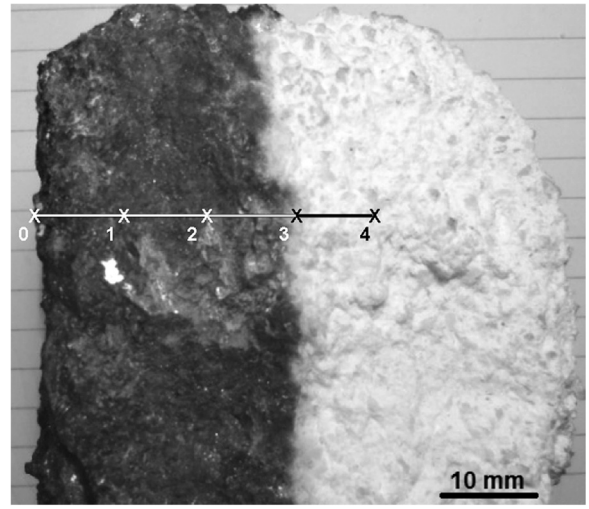

Fig. 1. Post-mortem analysis of the spent refractory, showing slag penetration and the corrosion profile depth (chemical analysis shown in Table 1).

Table 1
Chemical composition (determined by EDX, expressed as oxide wt%) of the spent refractory as a function of the distance to the hot face, as seen in Fig. 1.

Oxide	Distance to hot face (mm)				
	Hot face	Dark region		Interface	White region
	0	10	20	30	40
Al_2O_3	53.5	68.0	71.6	72.6	78.6
MgO	7.4	13.2	15.1	16.0	18.7
SiO_2	15.9	9.8	8.8	8.3	1.3
Na_2O	1.4	1.9	4.5	2.7	1.4
Fe_2O_3	7.4	6.5	–	0.4	–
MnO	11.8	–	–	–	–
TiO_2	1.5	–	–	–	–
Others	1.2	0.5	–	–	–

Table 2
Physical properties of the finer fractions (matrix) of the commercial raw material (RA) and the recovered waste materials (RN and RT).

Raw material	Density (g/cm^3)	Matrix PSD		
		d50 (μm)	d90 (μm)	SSA (cm^2/g)
RA	3.92	15.9	33.8	2288
RN	3.79	18.3	35.3	2257
RT	3.69	16.3	34.2	2389

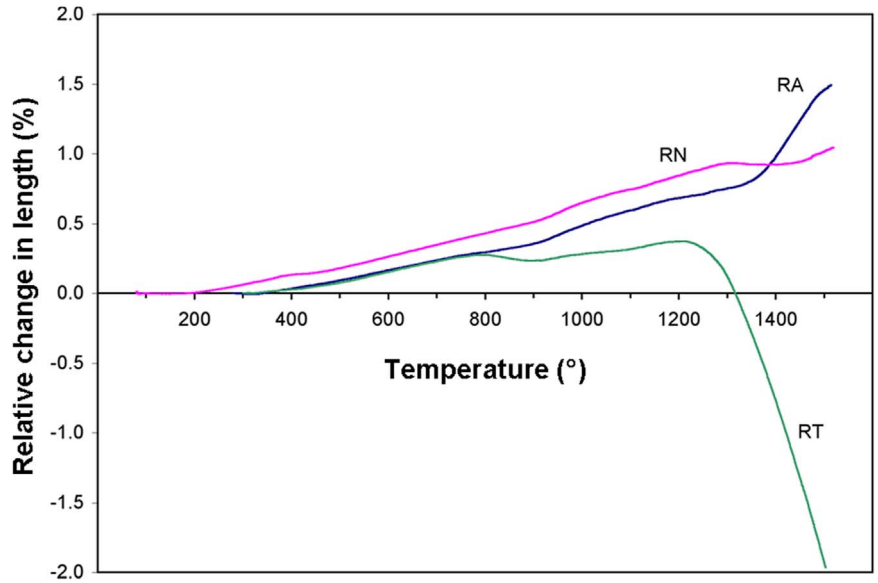

Fig. 2. Comparison of the dilatometric behaviour of the commercial raw material (RA) and the recovered waste materials (RN and RT).

mined for all sintered test-pieces using Archimedes water displacement method (ASTM C20).

Changes in the mineralogy due to chemical composition (contamination) and sintering temperature were determined by powder X-ray diffraction (XRD, Rigaku DMAX III1C, Cu Kα radiation). Polished sintered samples were observed by SEM-EDX, after carbon coating.

As an alternative to the colour-based manual separation, other procedures were experimented, namely density based mechanic vibration and magnetic separation. To better assess the efficiency of the separation processes, powder mixtures were evaluated in three size classes: "less than 100 μm" (d_{50}=4.51 μm); "less than 850 μm" (d_{50}=351 μm) and "higher than 1180 μm" (d_{50}=1977 μm). For the separation by mechanic vibration two glass containers with different diameters (150 and 50 mm) and three vibration amplitudes (1.5, 1.75 and 2.0 mm/s, for 30 min) were used. For the magnetic separation technique, applied to the same particle size classes, a neodymium permanent magnet ($Nd_2Fe_{14}B$, K & J Magnetics) was used and the separation efficiency was quantified by XRD and SEM-EDX.

After magnetic separation, the coarse and medium particle size classes were used to produce new self-flowing (q≈0.22) and vibratable (q≈0.26) castables. The new castables were composed to include a clean matrix containing reactive (CT3000SG) and tabular (T60) aluminas, as well as a fine particle size class obtained from RA. The amounts of each size class, to prepare 2 kg batches, were calculated with EMMA [25]. Calcium aluminate cement CA25 was used as binder (1 wt%) with two added-water levels (0.160 and 0.175 $g_{water}/m^2_{mixture\ SSA}$) and citric acid (0.05 wt%) as deflocculant. The flowability index (FI) was determined for dry and wet powder mixtures (ASTM C230).

Test-pieces were cast (150×25×25 mm^3) in stainless steel moulds and left to rest at room temperature for 24 h, then dried (110 °C, 24 h) and sintered at 1350 and 1500 °C. Sintered test-pieces were characterized in terms of XRD, SEM-EDX, dynamic Young's modulus E_{dyn} by ultrasonic pulse velocity (BS 1881) and mechanical (ASTM C133) and physical (ASTM C20) behaviour, as described previously.

3. Results and discussion

3.1. Evaluation of the reuse potential of spent linings

The chemical composition of a typical spent refractory fragment (post-mortem analysis) was determined as a function of the distance perpendicular to the hot "dark" face, on the five regions marked as shown in Fig. 1, to find out the oxide penetration depth profile. The analyses results, presented in Table 1, are approximate and serve only for comparison purposes. It can be observed that, as the distance to the hot face increases (from "dark" to "white" region), the slag penetration decreases and, as a consequence, the alumina and magnesia contents increase while the silica content decreases. It can be seen that the refractory in the cold "white" face region does not differ much from the nominal 86 wt% Al_2O_3 and 13 wt% MgO indicated for RA by the supplier, with a slight increase in the SiO_2 content, whereas that in the hot "dark" face region clearly shows the silica pick-up and loss of magnesia.

The existing temperature gradient across the lining thickness during service also results in differences in the extent of sintering, the cold "white" face region being more friable. This and the slag impregnation, result in mechanical strength mismatch between the two coloured regions, which helps the separation of the refractory fragments into material lots with different colour and chemistry. Thus, the two regions could be manually separated and a second type of sample was produced, besides the global indiscriminate sample (composed of both "white" and "dark" regions): a less-contaminated sample (cold "white" face only), with low silica content. The effect of slag contamination and impurities level on properties can thus be compared relative to the virgin raw material used in the original lining.

The particle size distribution of the commercial raw material (RA) is bimodal, with a coarse fraction of particles larger than 1180 μm (~38 wt%) and a matrix fraction of particles finer than 63 μm (~62 wt%). For bimodal particle size distributions, the matrix fraction is the key controlling-factor in the overall castable performance. The PSD modulus q, as defined by the Andreasen theory (cumulative percentage of particles finer than D, $CPFT=100\times(D/D_L)^q$, where D_L is the size of the largest particle in the distribution), provides a good estimate of the particles packing efficiency, best packing corresponding to a q value between 0.33 and 0.5 whereas easiest flow corresponds to q values close to 0.22 [25]. To enable comparison of properties (rheological behaviour, flowability index and workability), the PSD of the two types of recovered materials were adjusted using EMMA to reproduce that of RA, whose Andreasen modulus is q=0.79 (Table 2). The two new all-waste refractory powder mixtures with designed PSD were labelled RT (global indiscriminate refractory powder) and RN (less-contaminated refractory powder). Table 2 compares the major physical properties of the finer fractions (matrix) of the three powders RA, RT and RN.

From the dilatometry tests (Fig. 2) it can be seen that there are no

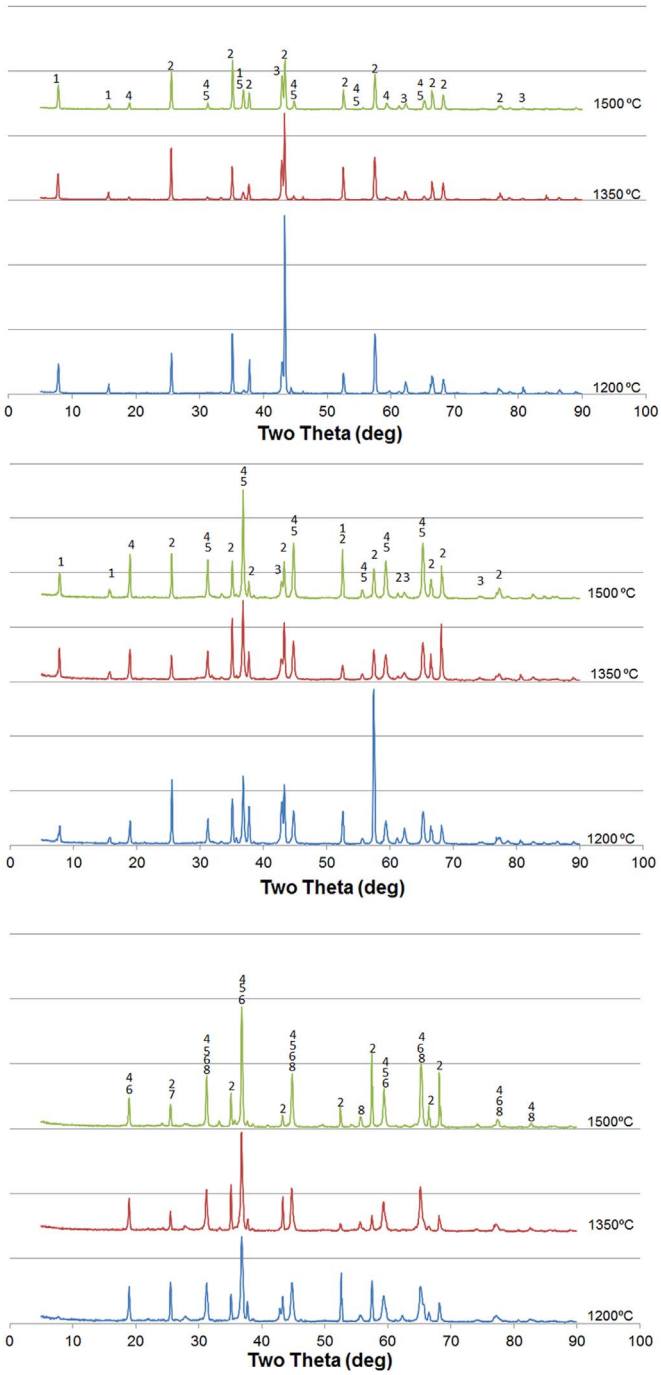

Fig. 3. X-ray diffraction patterns obtained for the refractories prepared with RA (top), RN (middle) and RT (bottom), as a function of the sintering temperature. Legend: 1- sodium aluminium oxide ($Na_2Al_2O_3$), 2- corundum (Al_2O_3), 3- periclase (MgO), 4- spinel ($MgAl_2O_4$), 5- ringwoodite ($(Mg,Fe)_2SiO_4$), 6- iron oxide (Fe_2O_3), 7- aluminium tungsten oxide (Al_xWO_3), 8- Strontium tin oxide ($SrSnO_3$).

significant differences in the thermal expansion coefficients of RA and RN up to ~1300 °C (and even of RT up to 800 °C). In RA, the expansive formation of magnesium aluminate spinel can be seen near 1350 °C, as the result of the reaction between aggregates (mainly alumina) and the magnesia from the matrix. Given that the recovered material has already been exposed to the furnace operating temperature, such expansion is hardly visible in the dilatometric curve of RN. As for the sample RT, with higher contamination level, the effect of the presence of fluxing impurities (particularly SiO_2, Na_2O and Fe_2O_3) can be seen from 800 °C upwards (on-set of densification) followed by significant shrinkage above 1200 °C.

Fig. 3 presents the observed changes in mineralogy (XRD patterns) due to changes in chemical composition and sintering temperature (1200, 1350 and 1500 °C). From the XRD patterns, it can be seen that spinel starts developing in RA at 1350 °C, as suggested by the dilatometry. Also confirming the dilatometry, spinel is already present in RN and RT at lower temperatures (1200 °C). Nevertheless, the mineralogy of RN is rather similar to that of RA, whereas the XRD pattern of RT reveals the presence of various foreign phases resulting from the impurities.

Fig. 4 shows the firing linear change as the sintering temperature increases. A similar trend towards expansion can be observed for RA and RN. This tendency is certainly due to the spinel expansive formation but can also result from the rather high q value of the matrix (the lower the q values, the higher the shrinkage). The counteracting effect of fluxing impurities in the more contaminated sample RT can clearly be observed from 1350 to 1500 °C.

The three-point bending modulus of rupture (MoR) and compressive strength results for the three sintered compositions are shown in Fig. 5. The rise in mechanical strength values as the sintering temperature increases, either in bending or in compression, is a consequence of the sintering progress. At any given sintering temperature, the values obtained for the refractories prepared with recovered materials (RN and RT) are always higher than those for the commercial raw material RA. The difference between the values for RA and RN might be explained by the expansive formation of spinel in RA (as seen in the XRD patterns), which weakens the microstructure. The much higher values registered for RT most likely are the result of the glassy phase bonding that develops during cooling of the liquid formed from the silicates and fluxing impurities.

Fig. 6 presents the variations in bulk density and apparent porosity as the sintering temperature increases. The expansive formation of spinel results in a decrease in bulk density and an increase in apparent porosity when the sintering temperature increases and its effect can be best seen in RA, in which spinel formation is more important. Contrariwise, the effect of the formation of a liquid phase during sintering, expected to be particularly abundant at 1500 °C, is clearly evident in the nearly constant properties of RT.

These preliminary results show that the un-sorted spent refractory RT, with a high level of contamination, cannot be used as such in future refractory applications. However, the fraction with lower contamination level, RN, with good physical, mechanical and structural properties, configures a strong possibility of being re-used as a refractory material. However, an efficient colour-based recycling process entails a laborious waste selection and separation work, which is, from an economic point of view, rather unattractive and rouses no sympathy. Therefore, anticipating the economical constraints that a manual colour-based sorting operation would bring into an industrial waste separation process, alternative partial decontamination procedures for RT were evaluated.

3.2. Alternative partial decontamination procedures

To better assess the efficiency of the separation processes, powder mixtures of the global indiscriminate refractory waste, extending from the cold to the hot face ("white" and "dark" regions) were evaluated in three size classes, fine (< 100 μm), medium (< 850 μm) and coarse (> 1180 μm). For the density-based separation by mechanic vibration, the motion of the particles could be observed in all the three size classes but without a clear particle separation (recognisable by colour difference). The method was, therefore, abandoned.

Fig. 7 illustrates how the magnetic separation of particles progresses as the average particle size of the three particle classes increases. It is clear that the contaminated volume removed from coarse particles is much higher (> 14 wt%), than that removed from medium (~3 wt%) and finer classes (< 2 wt%). This first analysis contributes decisively to an important conclusion: for any given

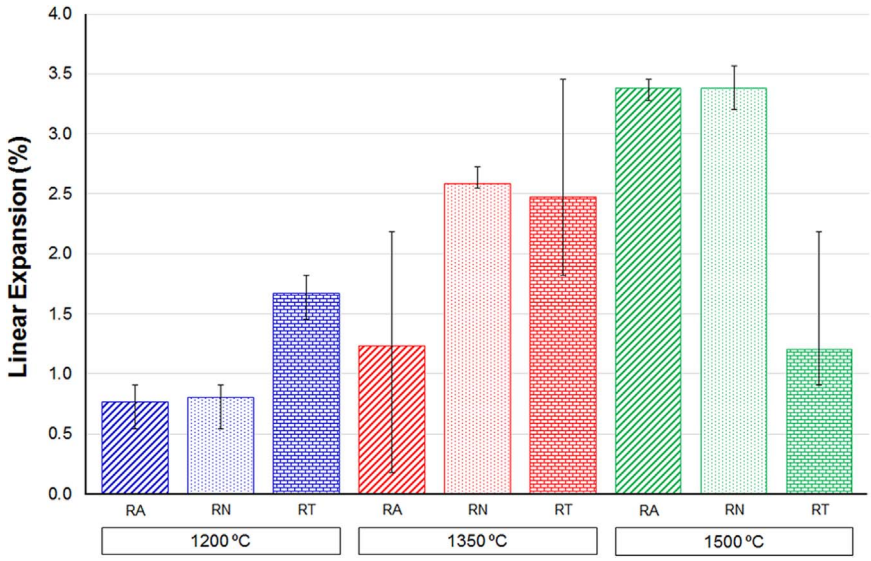

Fig. 4. Firing linear change of refractories prepared with the commercial raw material (RA) and the recovered waste materials (RN and RT), as a function of the sintering temperature.

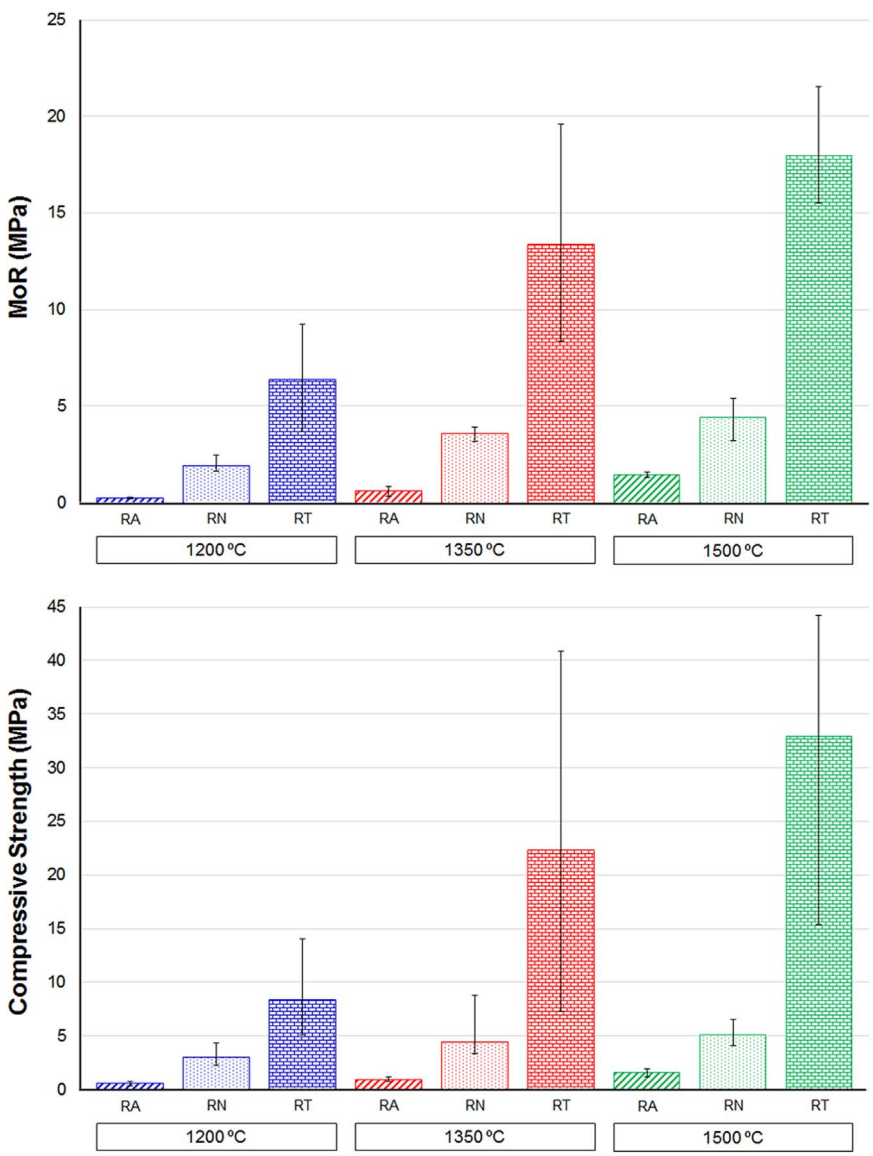

Fig. 5. Mechanical properties of sintered refractories prepared with the commercial raw material (RA) and the recovered waste materials (RN and RT), as a function of the sintering temperature: three-point bending MoR (top) and compressive strength (bottom).

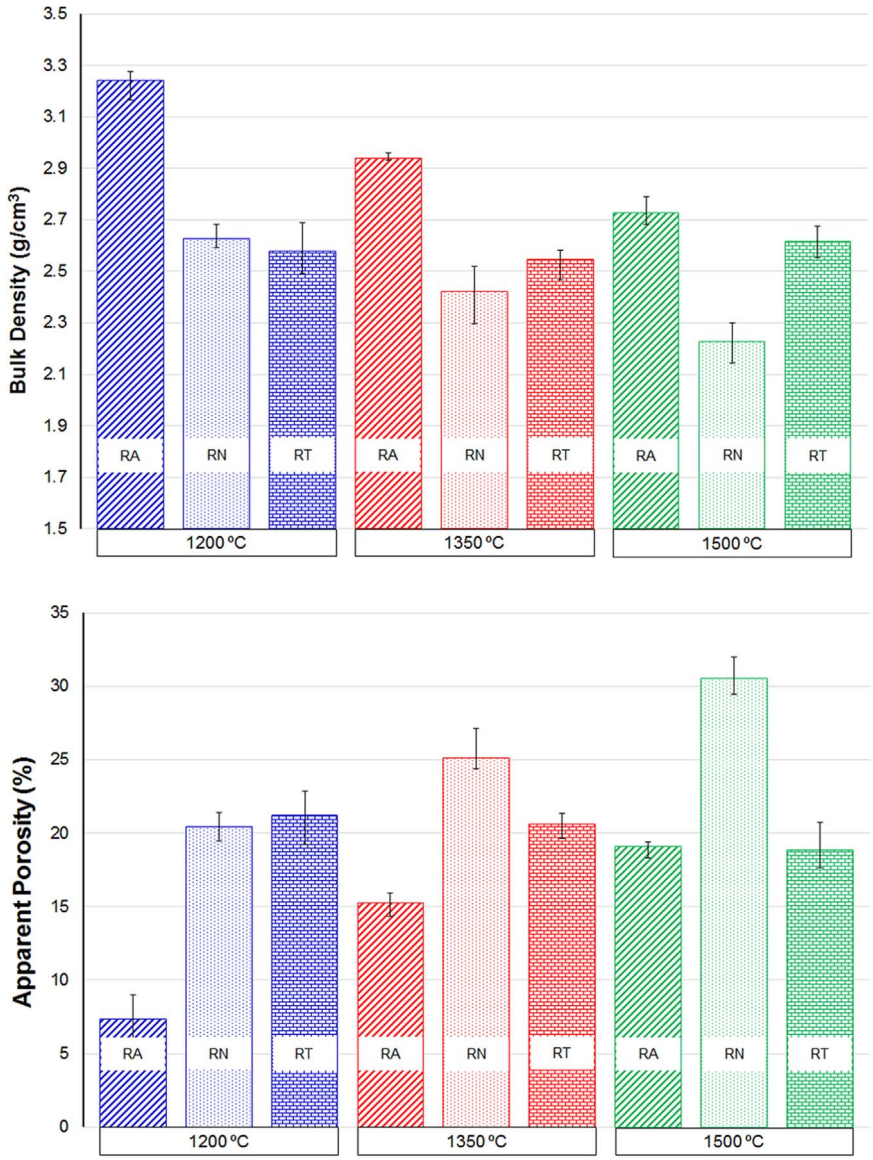

Fig. 6. Changes in bulk density (top) and apparent porosity (bottom) of sintered refractories prepared with the commercial raw material (RA) and the recovered waste materials (RN and RT), as a function of the sintering temperature.

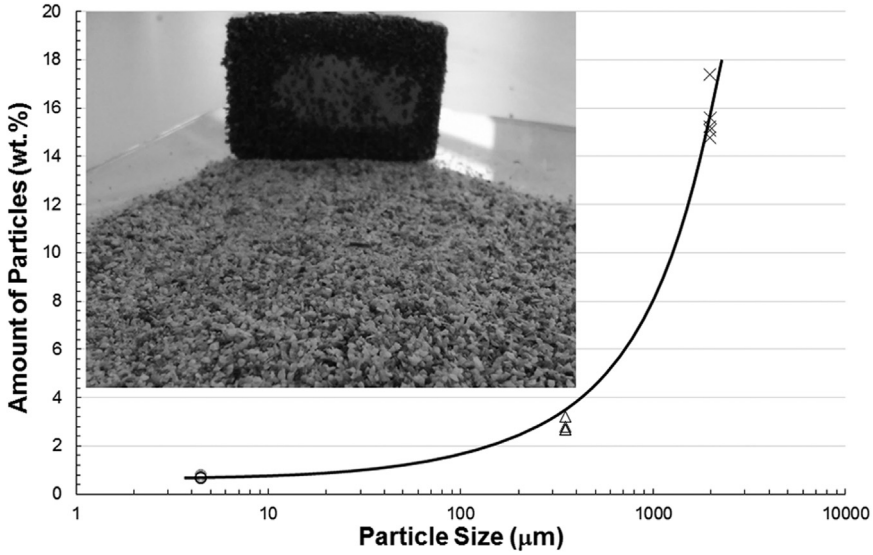

Fig. 7. Magnetic separation efficiency: amount of contaminated particles removed as a function of the average particle size in the starting powders.

Table 3
Chemical composition (determined by XRD and EDX, expressed as oxide wt%) of the magnetically separated powders (cleaner, less contaminated fraction not picked-up by the magnet, versus more contaminated fraction, picked-up by the magnet) as a function of the starting particle size.

	Cleaner fraction			Picked-up fraction		
	Coarse > 1180 μm	Medium < 850 μm	Fine < 100 μm	Coarse > 1180 μm	Medium < 850 μm	Fine < 100 μm
Al_2O_3	83.0	68.9	77.6	65.6	61.2	39.8
MgO	8.7	22.7	12.9	14.2	9.9	10.8
SiO_2	7.5	6.2	2.1	11.0	6.2	7.6
Na_2O	0.8	0.4	0.7	1.2	1.3	1.4
CaO	–	1.8	0.3	–	–	–
Fe_2O_3	–	–	0.8	0.7	14.5	30.4
MnO	–	–	5.6	7.3	6.9	4.6
Cr_2O_4	–	–	–	–	–	3.9
NiO_2	–	–	–	–	–	1.5

Table 4
Physical properties of the raw materials used in the design of new castables.

Raw material	Density (g/cm^3)	d50 (μm)	d90 (μm)	SSA (cm^2/g)
CA25	3.56	4.42	11.5	6799
CT3000SG	3.90	0.88	5.06	15293
T60 (< 200 μm)	3.79	85.5	185.2	729.4
Fine RA (< 100 μm)	3.79	16.82	40.67	2202
Medium size RC (< 850 μm)	3.47	351	834	161
Coarse size RC (> 1180 μm)	3.62	1977	3600	0.491

amount of contamination, although fine particles might lead to a more selective separation and the rejection of less material, the separation of contaminated particles gets harder (i.e. more laborious and time consuming) as the particle size gets finer. Therefore, the use of coarse particles is more attractive, not only due to a faster separation but also from an economic point of view because of the underlying reduced milling time.

Table 3 compares the composition (XRD and EDX) of the magnetically separated powders (cleaner, less contaminated fraction not picked-up by the magnet, versus more contaminated fraction, picked-up by the magnet). Only the coarse and medium size classes generate cleaner fractions with low level of metal contamination, expressed as Fe_2O_3, Cr_2O_3 and MnO. Nevertheless, these fractions still present relevant contents of SiO_2 (6.2–7.5 wt%) and Na_2O (0.4–0.8 wt%), which cannot be magnetically separated.

Table 5
Composition of the self-flowing (q=0.22) and vibratable (q=0.26) castable powder mixtures in terms of raw materials used (wt%).

	Raw material	q=0.22	q=0.26
Matrix	CA25	1.0	1.0
	CT3000SG	26.50	18.18
	T60	10.20	7.70
	Fine RA	15.31	14.34
	Total matrix	53.01	40.69
Aggregate	Medium size RC	25.52	30.61
	Coarse size RC	21.47	28.70
	Total aggregate	46.99	59.31

Table 6
Flowability Index (FI) of dry and wet castable powder mixtures.

	FI (dry) (%)	Added water ($g_{water}/m^2_{mixture\ SSA}$)/($g_{water}/g_{mixture}$)	FI (wet)[a] (%)
q=0.22	93	0.160/0.073	44
		0.175/0.080	88
q=0.26	72	0.160/0.053	0
		0.175/0.057	4

[a] After adding water and mixing in mortar mixer.

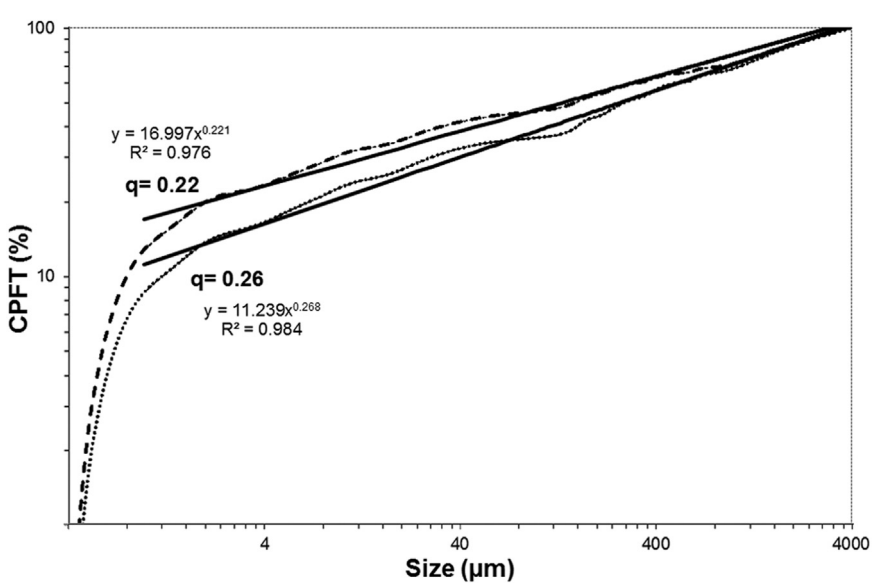

Fig. 8. PSDs of the self-flowing (q=0.22) and vibratable (q=0.26) castable powder mixtures.

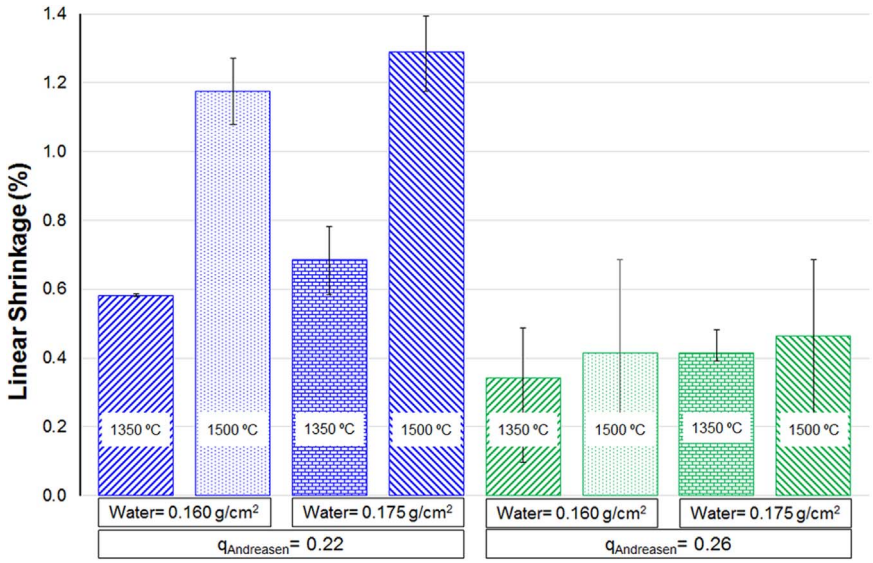

Fig. 9. Firing linear change of the self-flowing (q=0.22) and vibratable (q=0.26) castables, as a function of the added-water content and sintering temperature.

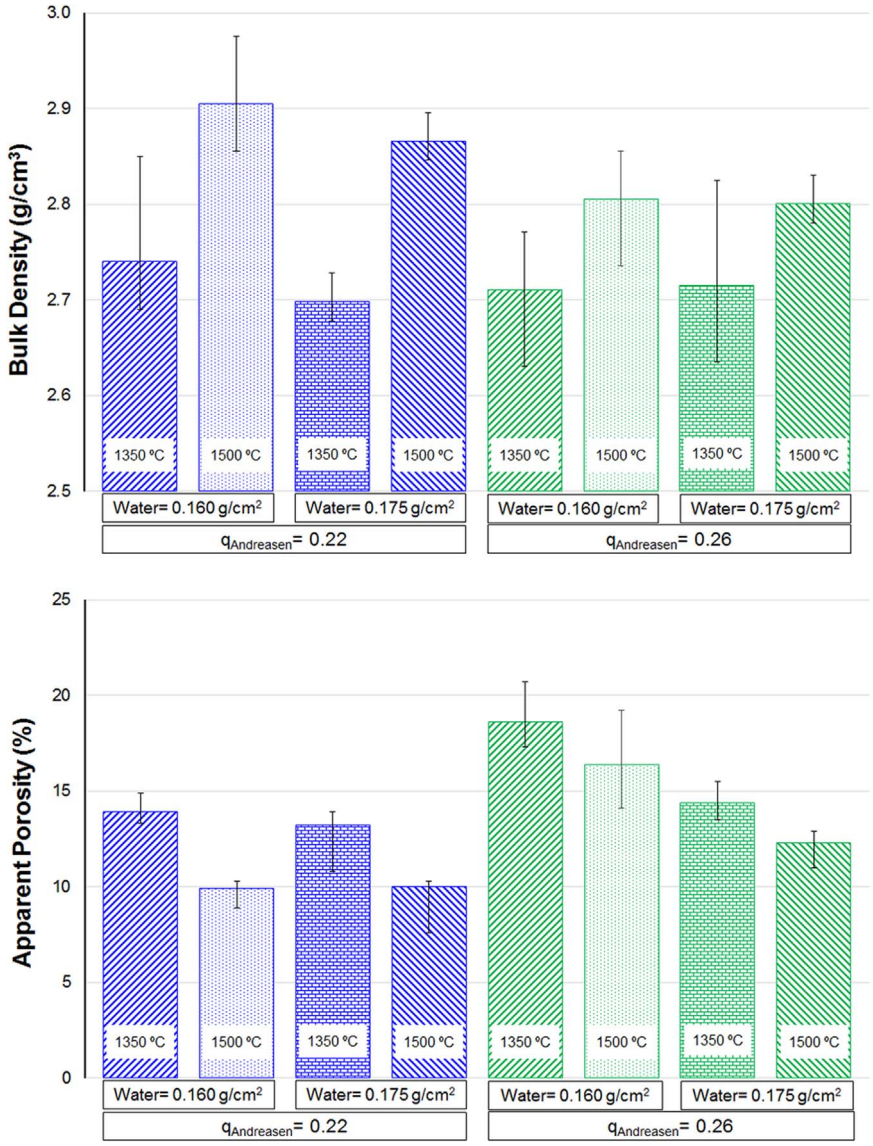

Fig. 10. Changes in the bulk density (top) and apparent porosity (bottom) of the self-flowing (q=0.22) and vibratable (q=0.26) castables, as a function of the added-water content and sintering temperature.

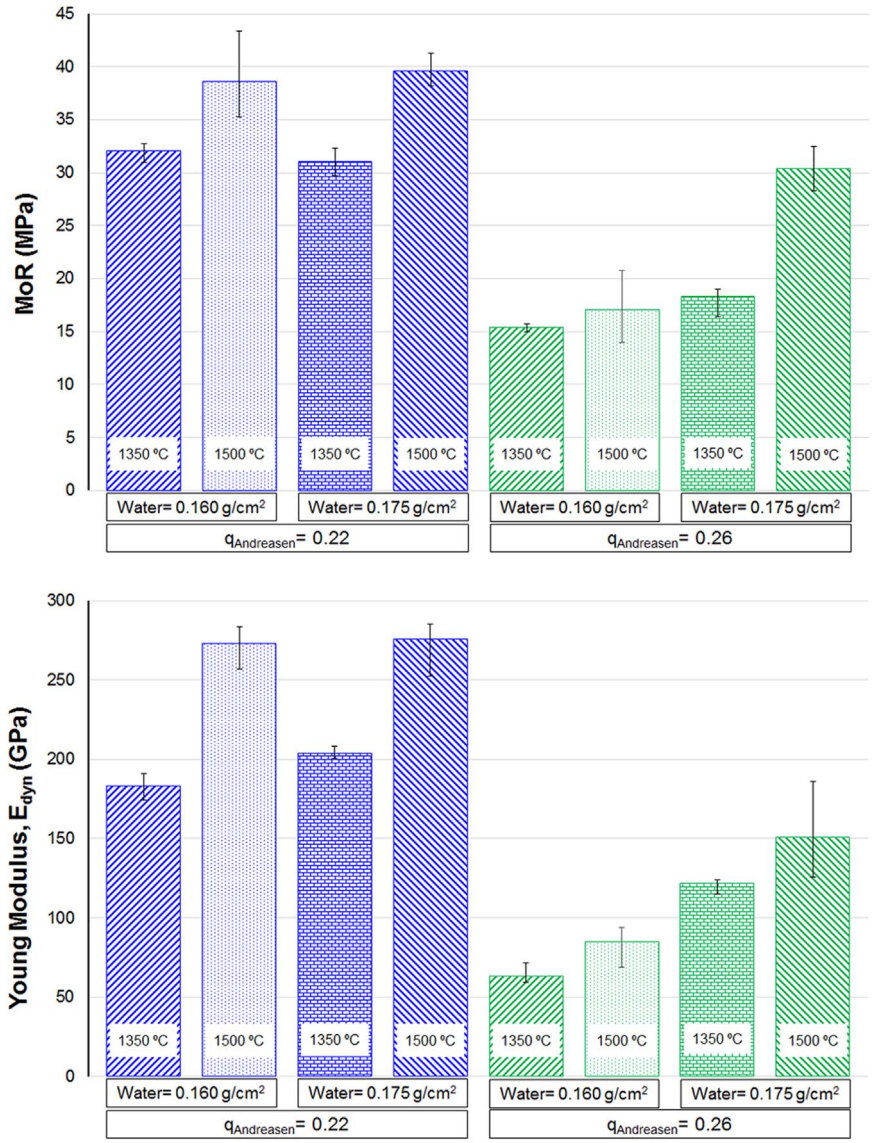

Fig. 11. Changes in three-point bending MoR (top) and stiffness (Young's modulus) (bottom) of the self-flowing (q=0.22) and vibratable (q=0.26) castables, as a function of the added-water content and sintering temperature.

Based on the above, it is envisaged that the cleaned coarser fractions of the spent refractory, labelled RC, might be used as aggregate in the design of new refractory castables. Combined with a fresh (virgin) matrix of finer particles, which are much more reactive than the aggregates and should be more resistant to corrosion [26], this also configures an attractive compromise reuse solution.

3.3. Design of new castables

As mentioned before, the matrix PSD is the key controlling-factor in the castable performance and the "natural" matrix fraction of RA (Table 2) has a rather high q value. To design the fresh (virgin) matrix of fine particles, fine grain reactive (CT3000SG) and tabular (T60) aluminas, as well as a class of fine particles obtained from RA, were used. The medium and coarse size classes of RC were used as aggregate. Table 4 shows the relevant properties of the raw materials used in the design of new castables.

To foresee eventual limitations due to the castable installation method, two powder mixtures with different Andreasen distribution modulus (a lower q value results in higher flowability index) were designed so that self-flowing (q≈0.22) and vibratable (q≈0.26) castables could be compared [25–28]. The PSDs were calculated with EMMA and are presented in Fig. 8. The amount of recycled material (RC waste after magnetic cleaning) used is ~47 wt% in the self-flowing castable and ~59 wt% in the vibratable castable (Table 5).

Although the Andreasen distribution modulus has a strong bearing on the flowability of the particulate system, the latter can be significantly altered when the added-water content is changed. Higher water contents promote the increase in flowability index (FI) and result in better workability, hence, easier application, but can have dire consequences on dried and fired properties [25,28]. Two quite different levels of added-water were chosen: the lower value of 0.160 $g_{water}/m^2_{mixture\ SSA}$ is the minimum necessary to wet the particles surface (corresponding to minimum flowability) while 0.175 $g_{water}/m^2_{mixture\ SSA}$ allows the presence of free water in the system [25,29]. For the chosen q values, the same water level, when expressed in terms of particles total specific surface area, translates into quite different values if expressed in a weight basis, due to the differences in particle sizes. This is shown in Table 6, which also shows the FI of the resulting dry and wet powder mixtures. The powder mixture designed to be self-flowing always shows higher FI, when compared to the vibratable mixture. For each mixture, the effect of extra added-water is also the expected one, i.e. higher FI. In any case, given the low water levels used, the drying linear change is always insignificant.

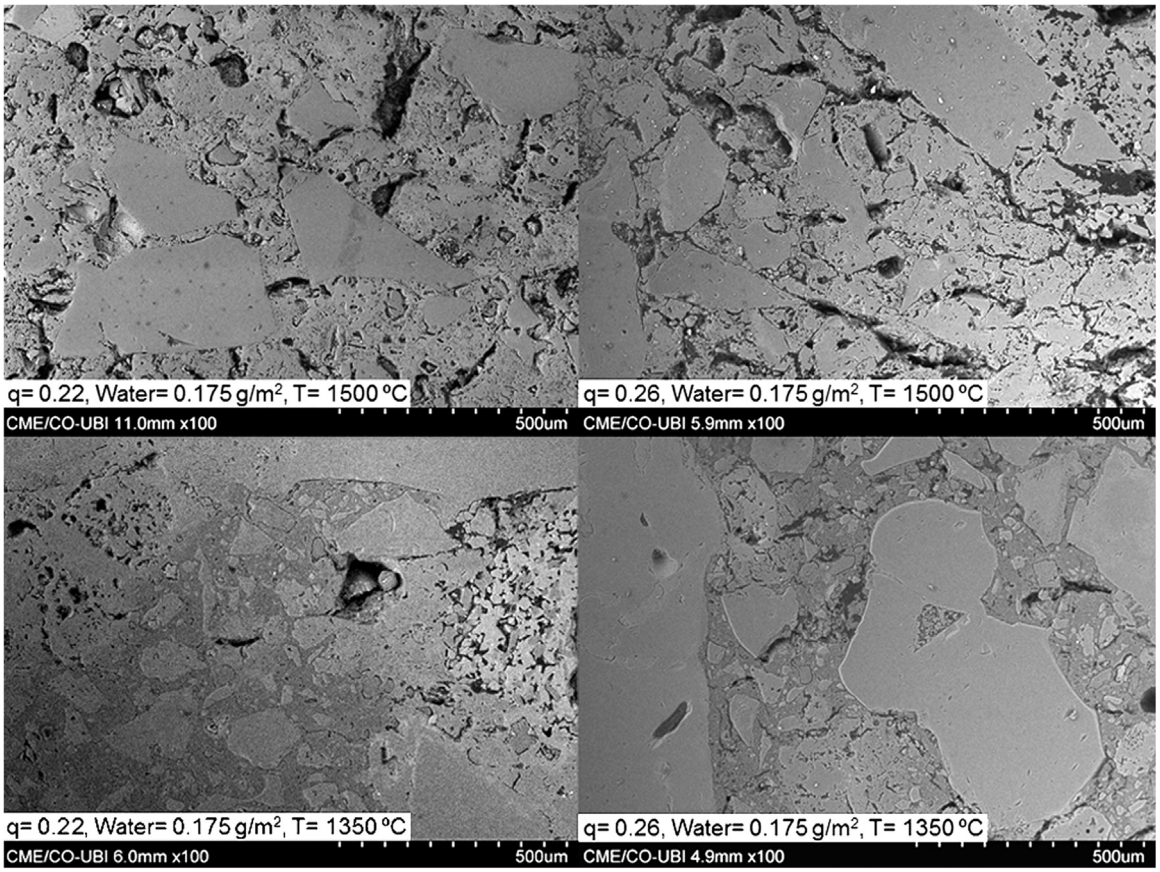

Fig. 12. Low magnification SEM micrographs of polished fracture surfaces of the self-flowing (q=0.22) and vibratable (q=0.26) castables sintered at 1350 and 1500 °C.

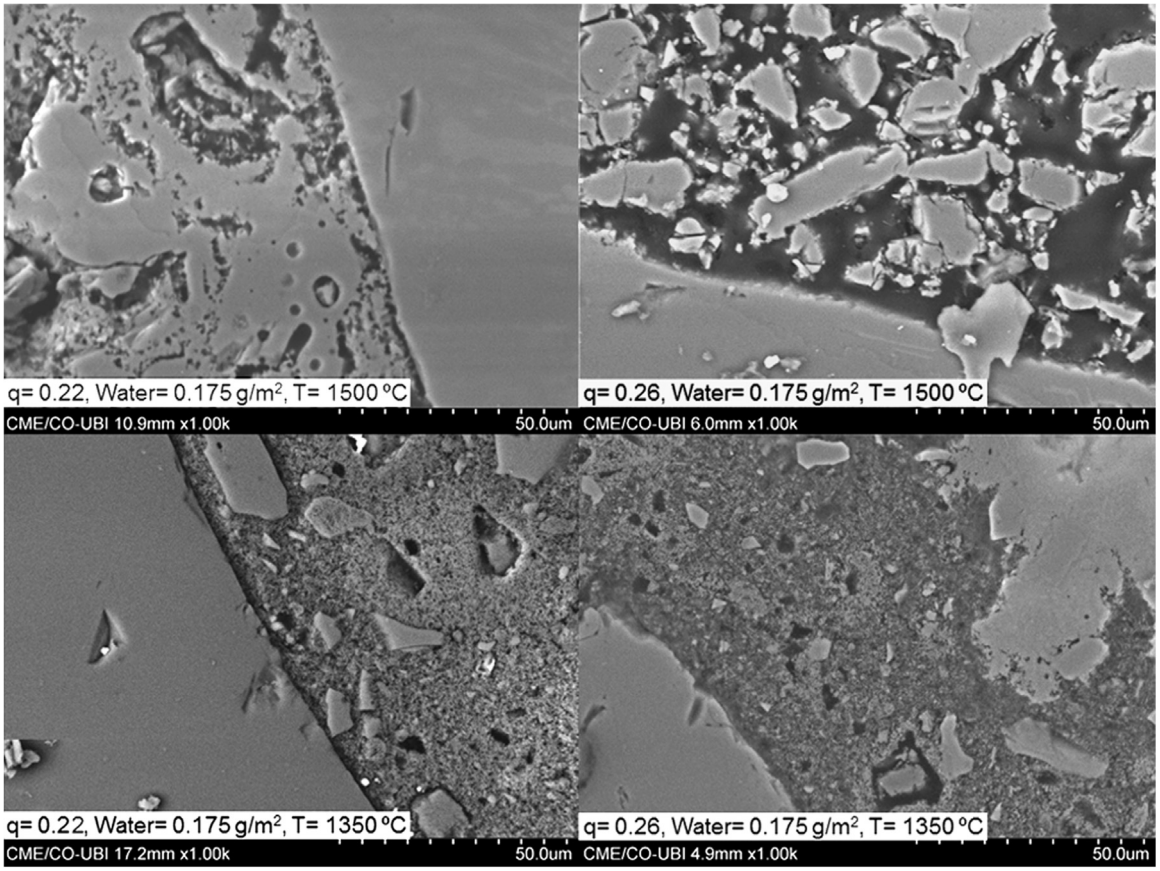

Fig. 13. High magnification SEM micrographs of polished fracture surfaces of the self-flowing (q=0.22) and vibratable (q=0.26) castables sintered at 1350 and 1500 °C.

Due to the designed PSD, all cast test-pieces show some shrinkage upon firing, generally lower than 1% (Fig. 9). Firing at 1500 °C results in higher shrinkage values, more so for higher added-water contents. As expected, the increase of the PSD Andreasen modulus from 0.22 to 0.26 translates into a ~40% reduction of the linear shrinkage at 1350 °C and ~64% at 1500 °C.

Fig. 10 shows the changes in the bulk density and the apparent porosity of the sintered castables. The usual increase in density and decrease in porosity as the sintering temperature increases from 1350 to 1500 °C can be observed. It is interesting to note that, when the particle sizes are designed for self-flow (q=0.22), promoting maximum paste thickness (MPT) and minimum interparticle separation (IPS) [25,28], the extra added-water has a stronger effect on density than on apparent porosity, which suggests that residual water remains entrapped in closed pores. On the contrary, for the vibratable castable (q=0.26) increasing the water content results in less porosity but no significant changes in bulk density. Apparently, in this case, additional water compensates for the lower flowability of the powder mixture (with higher q value) and contributes to a better mixture homogenization and workability. This results in better particle packing and the mechanical performance after firing is improved, as seen in Fig. 11.

Fig. 11 shows that the flexural strength (MoR) and the stiffness (Young's modulus) behave similarly, both increasing with the sintering temperature and reaching significantly higher values for the self-flowing castables (q=0.22), as compared to the equivalent vibratable ones (q=0.26). Again, the mechanical performance after firing is less affected by changes in added-water content in the self-flowing system.

Low magnification SEM micrographs of polished fracture surfaces are shown in Fig. 12. Despite the increase in bulk density with the sintering temperature and associated decrease in apparent porosity, a degradation of the matrix can be observed in the micrographs at 1500 °C. In both cases, the matrix shows a large number of microcracks, which might just be the consequence of a more difficult fracture (shattering) of stronger and stiffer samples.

The propagation of those microcracks in the matrix and the good interface bond between aggregate and matrix is illustrated in the high magnification SEM micrographs of Fig. 13. These observations suggest that further benefits can be gained if the matrix chemical composition is also adjusted to match that of the recovered aggregate, improving their mutual compatibility.

4. Conclusions

In this work, the reuse potential of spent refractories from dismantled steel melting induction furnace linings was investigated. Firstly, the collected material was colour sorted in two fractions, to compare the effect of contamination on properties relative to the virgin raw material used in the original lining. The results of this preliminary study showed that the un-sorted spent refractory, with a high level of contamination, can not be used as such in future refractory applications, whereas the less contaminated ("white" cold face only) fraction presented good physical, mechanical and structural properties, configuring a strong possibility of being re-used.

Anticipating the economical constraints that a manual colour-based sorting operation would bring into an industrial waste separation process, the spent refractory debris was then ground as a whole (white and dark fractions together), divided into three particle size classes (fine, medium and coarse) and subjected to magnetic separation. The obtained results showed that magnetic cleaning of coarse particles is more efficient which, from an economic point of view, is also more attractive because of the underlying reduced milling time. Therefore, such coarser fractions (with lower contamination level) were used as aggregate in the design of new self-flowing and vibratable castables (Andreasen PSD modulus q=0.22 and q=0.26, respectively) combined with a fresh (virgin) alumina-based matrix of finer particles. The designed PSDs enabled the use of large contents of recycled material (47 and 59 wt%, respectively).

Also, two different levels of added-water were chosen: a low value just enough to wet the particles surface and a higher one to guarantee the presence of some free water in the system (0.160 and 0.175 $g_{water}/m^2_{mixture\ SSA}$, respectively).

The obtained results showed that, despite the drastic reduction in wet flowability of the vibratable castable, the mechanical performance after firing is not unduly hindered when the q value or the added-water content increase. The self-flowing castable, which always presents a superior performance and is also less affected by changes in added-water content, presented a remarkable performance: 88% flowability index as wet paste, 1.29% linear shrinkage upon firing at 1500 °C, as well as 10% apparent porosity, 39.6 MPa bending strength and 276 GPa dynamic Young's modulus.

The results from this work demonstrate that landfilling (and the corresponding costs) of spent spinel-bonded high-alumina linings can be largely reduced by up grading the refractory scrap to secondary raw material through coarse grinding and magnetic separation of major impurities. Because it has already been exposed to high service temperature, this recovered raw material retains the microstructural distribution of in situ spinel formation without the corresponding disruptive expansion, mirroring the use of pre-formed spinel without the onus of a pre-firing. As such, it is capable of withstanding high temperatures and can be directly used in refractory applications such as furnace safety linings, core casting and casting accessories, to name a few.

References

[1] C.E. Semler, Refractories – The world's most important but least known products, Am. Ceram. Soc. Bull. 93 (2014) 34–35.
[2] C.E. Semler, The advancement of refractories technology never stop, Refract. World Forum 6 (2014) 27–35.
[3] E. De Guire, Refractories - engineered, high-performance "silent partners", Am. Ceram. Soc. Bull. 94 (2015) 26.
[4] K. Scharrer, Editorial, Refract. World Forum 5 (2013) 1.
[5] European Commission, Critical raw materials for the EU – Report of the Ad-hoc Working Group on Defining Critical Raw Materials, May update, 2014. Available online at: 〈http://ec.europa.eu/enterprise/policies/raw-materials/files/docs/crm-report-on-critical-raw-materials_en.pdf〉.
[6] G. Tiess, Minerals policy in Europe: some recent developments, Resour. Policy 35 (2010) 190–198. http://dx.doi.org/10.1016/j.resourpol.2010.05.005.
[7] G. Buchebner, A. Kronthaler, W. Hammerer, Magnesia-carbon bricks made in Europe: challenges and solutions, in: Proceedings of the 13th Unified International Technical Conference on Refractories (UNITECR 2013), Victoria, Canada, ACerS, 2013, pp. 224–228.
[8] T. Drnek, M. Seelig, Resource efficiency - global context, european policy initiatives and responses of RHI, Berg. Huttenmann. Monatshefte 157 (2012) 156–159.
[9] H. Epstein, A low cost, sustainable source of alumina for thermal insulation, Refract. World Forum 5 (2013) 69–74.
[10] A. Volckaert, Raw materials for refractories: the european perspective, in: Proceedings of the 13th Unified International Technical Conference on Refractories (UNITECR 2013), Victoria, Canada, ACerS, 2013, pp. 1065–1068.
[11] V. Funari, R. Braga, S.N.H. Bokhari, E. Dinelli, T. Meisel, Solid residues from Italian municipal solid waste incinerators: a source for "critical" raw materials, Waste Manag. 45 (2015) 206–216. http://dx.doi.org/10.1016/j.wasman.2014.11.005.
[12] S.P. Raut, R.V. Ralegaonkar, S.A. Mandavgane, Development of sustainable construction material using industrial and agricultural solid waste: a review of waste-create bricks, Constr. Build. Mater. 25 (2011) 4037–4042. http://dx.doi.org/10.1016/j.conbuildmat.2011.04.038.
[13] M. Coronado, A.M. Segadães, A. Andrés, Combining mixture design of experiments with phase diagrams in the evaluation of structural ceramics containing foundry by-products, Appl. Clay Sci. 101 (2014) 390–400. http://dx.doi.org/10.1016/j.clay.2014.05.021.
[14] P. Korgul, D.R. Wilson, W.E. Lee, Microstructural analysis of corroded alumina–spinel castable refractories, J. Eur. Ceram. Soc. 17 (1997) 77–84. http://dx.doi.org/10.1016/S0955-2219(96)00073-8.
[15] L.A. Díaz, R. Torrecillas, A.H. de Aza, P. Pena, Effect of spinel on slag attack resistance of high alumina refractory castables, J. Eur. Ceram. Soc. 27 (2007) 4625–4631. http://dx.doi.org/10.1016/j.jeurceramsoc.2007.04.007.
[16] J.D. Smith, H. Fang, K.D. Peaslee, Characterization and recycling of spent refractory wastes from metal manufacturers in Missouri, Resour. Conserv. Recycl. 25 (1999) 151–169.
[17] K.S. Kwong, J.P. Bennett, Recycling practices of spent MgO-C refractories, J. Miner. Mater. Charact. Eng. 1 (2002) 69–78. http://dx.doi.org/10.4236/jmmce.2002.12005.

[18] S. Hanagiri, T. Matsui, A. Shimpo, S. Aso, T. Inuzuka, T. Matsuda, S. Sakaki, H. Nakagawa, Recent improvement of recycling technology for refractories, Nippon Steel Technical Report 98, 2008, pp. 93–98.
[19] H.N. Yoshimura, A.P. Abreu, A.L. Molisani, A.C. Camargo, J.C.S. Portela, N.E. Narita, Evaluation of aluminum dross waste as raw material for refractories, Ceram. Int. 34 (2008) 581–591. http://dx.doi.org/10.1016/j.ceramint.2006.12.007.
[20] K. Andrzej, L. Obszyńska, M. Sułkowski, The issue of use of basic refractory scrap, in: Proceedings of the 13th Unified International Technical Conference on Refractories (UNITECR 2013), Victoria, Canada, ACerS, 2013, pp. 1365–1370.
[21] A.P. Luz, D.O. Vivaldini, F. López, P.O.R.C. Brant, V.C. Pandolfelli, Recycling MgO-C refractories and dolomite fines as slag foaming conditioners: experimental and thermodynamic evaluations, Ceram. Int. 39 (2013) 8079–8085. http://dx.doi.org/10.1016/j.ceramint.2013.03.080.
[22] R. Otake, H. Sawada, K. Nakanishi, K. Kobayashi, Development of a monolithic refractory using spent refractories, in: Proceedings of the 13th Unified International Technical Conference on Refractories (UNITECR 2013), Victoria, Canada, ACerS, 2013, pp. 549–553.
[23] J. Poirier, Use of secondary alumina-graphite as raw material of alumina-graphite silicon carbide refractories, Refract. World Forum 5 (2013) 97–100.
[24] N. Malenšek, V. Ducman, B. Mirtič, Recycled granulate obtained from waste alumina-rich refractory powder by the cold bonding process, Ceram. Int. 41 (2015) 8996–9002. http://dx.doi.org/10.1016/j.ceramint.2015.03.214.
[25] A.P. Silva, D.G. Pinto, A.M. Segadães, T.C. Devezas, Designing particle sizing and packing for flowability and sintered mechanical strength, J. Eur. Ceram. Soc. 30 (2010) 2955–2962. http://dx.doi.org/10.1016/j.jeurceramsoc.2009.12.017.
[26] A. Obregón, J.L. Rodríguez-Galicia, J. López-Cuevas, P. Pena, C. Baudín, MgO-$CaZrO_3$-based refractories for cement kilns, J. Eur. Ceram. Soc. 31 (2011) 61–74. http://dx.doi.org/10.1016/j.jeurceramsoc.2010.08.020.
[27] A.R. Studart, R.G. Pileggi, J. Gallo, V.C. Pandolfelli, High-alumina multifunctional refractory castables, Am. Ceram. Soc. Bull. 80 (2001) 34–40.
[28] A.P. Silva, A.M. Segadães, T.C. Devezas, MPT influence on the rheological behaviour of self-flow refractory castables, Mater. Sci. Forum 587–588 (2008) 133–137. http://dx.doi.org/10.4028/www.scientific.net/MSF.587-588.133.
[29] A.P. Silva, T.C. Devezas, A.M. Segadães, Particle distribution design in a self-flow alumina refractory castable without cement, Adv. Sci. Technol. 45 (2006) 2260–2265. http://dx.doi.org/10.4028/www.scientific.net/AST.45.2260.